

Article

Influence of Substrate Temperature during In_xS_y Sputtering on $\text{Cu}(\text{In,Ga})\text{Se}_2$ /Buffer Interface Properties and Solar Cell Performance

Dimitrios Hariskos, Wolfram Hempel, Richard Menner and Wolfram Witte *

Zentrum für Sonnenenergie- und Wasserstoff-Forschung Baden-Württemberg (ZSW), 70563 Stuttgart, Germany; dimitrios.hariskos@zsw-bw.de (D.H.); wolfram.hempel@zsw-bw.de (W.H.); richard.menner@zsw-bw.de (R.M.)

* Correspondence: wolfram.witte@zsw-bw.de; Tel.: +49-711-7870-292

Received: 20 December 2019; Accepted: 31 January 2020; Published: 5 February 2020



Abstract: Indium sulfide (In_xS_y)—besides CdS and Zn(O,S)—is already used as a buffer layer in chalcopyrite-type thin-film solar cells and modules. We discuss the influence of the substrate temperature during very fast magnetron sputtering of In_xS_y buffer layers on the interface formation and the performance of $\text{Cu}(\text{In,Ga})\text{Se}_2$ solar cells. The substrate temperature was increased from room temperature up to 240 °C, and the highest power conversion efficiencies were obtained at a temperature plateau around 200 °C, with the best values around 15.3%. Industrially relevant in-line co-evaporated polycrystalline $\text{Cu}(\text{In,Ga})\text{Se}_2$ absorber layers were used, which yield solar cell efficiencies of up to 17.1% in combination with a solution-grown CdS buffer. The chemical composition of the In_xS_y buffer as well as of the $\text{Cu}(\text{In,Ga})\text{Se}_2/\text{In}_x\text{S}_y$ interface was analyzed by time-of-flight secondary ion mass spectrometry. Changes from homogenous and stoichiometric In_2S_3 layers deposited at RT to inhomogenous and more sulfur-rich and indium-deficient compositions for higher temperatures were observed. This finding is accompanied with a pronounced copper depletion at the $\text{Cu}(\text{In,Ga})\text{Se}_2$ absorber surface, and a sodium accumulation in the In_xS_y buffer and at the absorber/buffer interface. These last two features seem to be the origin for achieving the highest conversion efficiencies at substrate temperatures around 200 °C.

Keywords: indium sulfide; sputtering; CIGS; thin film; solar cell; buffer; ToF-SIMS; depth profile

1. Introduction

Indium sulfide (In_2S_3) is one of the materials, besides CdS and Zn(O,S), which is already used as a buffer layer in chalcopyrite-type solar modules [1,2]. Due to environmental concerns and the political decision to avoid Cd in solar modules, In_2S_3 could be a candidate of choice to apply as a buffer layer for $\text{Cu}(\text{In,Ga})\text{Se}_2$ (CIGS) thin-film solar cells instead of the established CdS. In_xS_y layers for the application as CIGS buffers can be grown by almost all available deposition techniques, including atomic layer deposition (ALD), thermal evaporation, chemical bath deposition (CBD), ion layer gas reaction (ILGAR), spray pyrolysis, and sputtering [3–5]. A value of 18.2% (with anti-reflective coating) was reported by Spiering et al. for a CIGS cell with thermal evaporated In_xS_y buffer [6], 17.9% (certified) was achieved with a 30 cm × 30 cm module with thermal evaporated $\text{In}_x\text{S}_y:\text{Na}$ buffer by the company Avancis [7], 16.4% were published for a cell with an ALD In_xS_y buffer [4], 16.8% (in-house) and 16.1% (certified) were achieved by Saez-Araoz et al. with an ILGAR $\text{In}_x\text{S}_y:\text{Cl}$ buffer [8], and 14.3% for a 225 cm² cell with a reactively sputtered $\text{In}_x(\text{O,S})_y$ buffer fabricated by the company Midsummer [2].

The sputtering approach can be easily implemented in an industrial environment, similar to the sputtering of the molybdenum back contact, high-resistive layers and transparent conductive oxides used as front contact. Furthermore, the method would be favorable compared to ALD, thermal

evaporation, or growth by CBD, due to the very fast deposition times of approximately one minute or less; compared to ten or even more minutes to deposit a 20–60 nm thick In_xS_y buffer layer. This “dry” sputtering process could be a candidate for an application in a roll-to-roll coater with a flexible substrate or the implementation in an in-line deposition machine without breaking the vacuum after CIGS absorber deposition.

We present our development of very fast rf-magnetron sputtered In_xS_y buffer layers deposited at different substrate temperatures, show the efficiency results of In_xS_y -buffered cells with open-circuit voltage (V_{OC}) values close to reference cells with CBD-CdS buffer, and discuss the influence of substrate temperature during In_xS_y sputtering. In addition, a detailed materials characterization of our various In_xS_y buffer layers including chemical depth profiles for the analysis of the In_xS_y buffer and CIGS/ In_xS_y interface reveal a sodium accumulation in the In_xS_y buffer and at the CIGS/buffer interface and a copper depletion of the CIGS surface with higher substrate temperatures.

2. Materials and Methods

Polycrystalline CIGS absorber layers with a thickness of 2.3 μm , a Ga/(Ga+In) ratio of 0.3 and a Cu/(Ga+In) of 0.8 were grown in an industrially relevant in-line multi-stage co-evaporation process on Mo-coated soda-lime glass [9]. No alkali post-deposition treatment was applied prior to the buffer deposition, which can significantly improve the device performance mainly due to an increased V_{OC} .

In the next step, In_xS_y as the buffer layer was rf-magnetron sputtered in a VON ARDENNE (Dresden, Germany) high-vacuum sputtering system of type CS 730S from a commercially available In_2S_3 target with a diameter of 20 cm in a pure argon atmosphere (for further details see [10]). The substrate temperature during sputtering of the In_xS_y layers was increased from room temperature (RT) up to 240 °C at low power densities of approximately 1 W/cm^2 compared to high power densities around 10 W/cm^2 typically used for ZnO:Al sputtering [11]. Thicknesses of In_xS_y buffer layers for solar cells were in the range of 30–60 nm for deposition times of 40–80 s, resulting in a sputter deposition rate of approximately 0.8 nm/s. In addition, around 500 nm thick In_xS_y layers were deposited on highly transparent suprasil quartz glass substrates for transmittance and grazing incident X-ray diffraction (GIXRD) measurements. The thicknesses of the thin In_xS_y layers were determined on CIGS/ In_xS_y cross-sections with a scanning electron microscope and for the thick layers by evaluation of the transmittance data. The commonly used CdS buffer with approximately 50 nm thickness was grown by CBD with a thiourea-based process as reference material.

Subsequently, rf-sputtered undoped ZnO (i-ZnO) was applied as high-resistive layer and dc-sputtered ZnO:Al served as front contact with Ni/Al/Ni grid fingers deposited by e-beam evaporation on top. The total cell area was 0.5 cm^2 . Figure 1a illustrates the stacking sequence as used in this work with a sputtered In_xS_y buffer in combination with i-ZnO. Alternatively we tried different stacking sequences with rf-sputtered $\text{Zn}_{0.75}\text{Mg}_{0.25}\text{O}$ as high-resistive layer instead of i-ZnO and without any high-resistive layer with ZnO:Al deposited directly on top of In_xS_y . Both approaches turned out fine but could not significantly improve the cell efficiencies compared to our standard stacking sequence with i-ZnO, which we used for the present work.

Current–voltage (I – V) curves were measured with a WACOM (Saitama, Japan) AM1.5G solar simulator with four-point geometry at standard testing conditions with a silicon reference solar cell for calibration. External quantum efficiency (EQE) measurements were performed with a BENTHAM (Berkshire, UK) PVE 300 setup with an additional light bias. For I – V and EQE measurements the CIGS cells were in the as-grown state (no further light-soaking or post-annealing procedures were applied). The transmittance of 500 nm thick In_xS_y layers on suprasil quartz glass substrates was measured with a Perkin Elmer (Waltham, MA, USA) UV/VIS/NIR Lambda 900 spectrometer and GIXRD patterns for structural characterization were obtained with a PANalytical (Almelo, The Netherlands) Empyrian diffractometer with Cu K_α radiation with an incident angle of 0.5°.

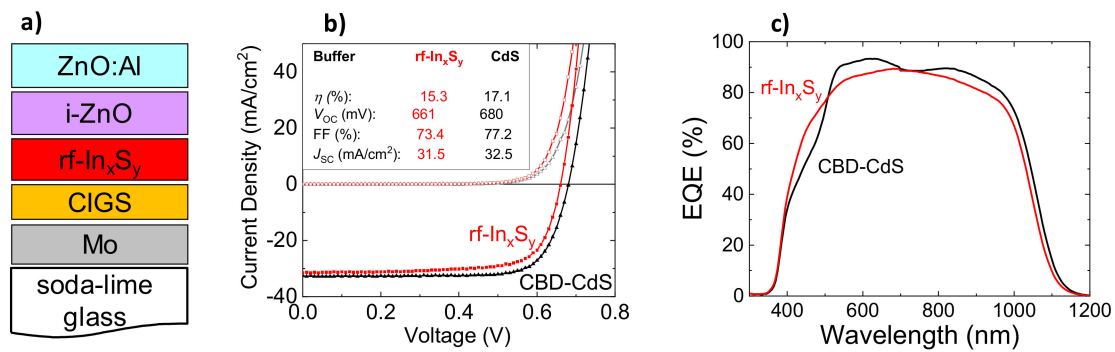


Figure 1. (a) Scheme of Cu(In,Ga)Se₂ (CIGS) thin-film solar cell with rf-sputtered In_xS_y buffer layer (not to scale); (b) *I*–*V* curves of CIGS solar cells either with rf-magnetron sputtered In_xS_y buffer at 220 °C substrate temperature (red) or with a CdS buffer layer (black) grown by chemical bath deposition (CBD), both with i-ZnO/ZnO:Al on top. Corresponding solar cell parameters are listed in the inset. *J*_{SC} values are corrected with EQE; (c) External quantum efficiency (EQE) curves of the same cells.

We performed time-of-flight secondary ion mass spectroscopy (ToF-SIMS) depth profiles with a ToF⁵-SIMS instrument from IONTOF (Münster, Germany). A Bi⁺ liquid metal gun running at 30 keV generates the secondary ions, which are recorded by a time-of-flight detector. We choose an oxygen gas gun as sputtering source to detect sodium in a good sensibility. To acquire quantified depth profiles of sulfur, oxygen, and CIGS matrix elements, we selected a cesium metal gun. Both sputter guns worked at an energy of 2 keV. The size of the sputter area with 130 × 130 μm² was larger than the analysis area of 80 × 80 μm² to get rid of crater edge information. For the quantified measurement, we chose an analysis area of 80 × 80 μm² and a sputter area of 500 × 500 μm² to increase the number of data points.

3. Results

3.1. Solar Cell Characteristics

3.1.1. Comparison of Sputtered In_xS_y- and CBD CdS-Buffered Solar Cells

Figure 1 depicts the *I*–*V* and EQE curves of the best In_xS_y- and CdS-buffered CIGS solar cells fabricated within this experimental campaign. The corresponding solar cell parameters are listed in the inset of Figure 1b. With 15.3%, the efficiency of the In_xS_y-buffered cell is reduced compared to the reference cell with CdS buffer with 17.1% efficiency—mainly due to a lower fill factor (FF). Nevertheless, the *V*_{OC} is only slightly lower with 661 mV compared to 680 mV of the reference cell. There is no gain in short-circuit current density (*J*_{SC}) for the In_xS_y-buffered cell as there is an absorption in the short wavelength region in the EQE (see Figure 1c). This feature is the result of a too-low bandgap energy and parasitic absorption due to the pronounced thickness of the In_xS_y layer. In addition, the EQE values of the In_xS_y-buffered cell are slightly below the CdS reference in the region between 500 and 1100 nm. The gradual decrease in EQE between 700 and 400 nm would tend to an indirect bandgap energy for In_xS_y. We observed no significant effect, neither positive nor negative, with cold-light soaking under AM1.5G conditions on solar cell parameters of CIGS solar cells with sputtered In_xS_y buffer.

3.1.2. Dependency of Solar Cell Efficiency on Substrate Temperature During In_xS_y Sputtering

Figure 2 shows the dependency of solar cell parameters on substrate temperature during sputtering of the In_xS_y buffer layer. Relatively low efficiency values resulted for cells with In_xS_y sputtered at RT whereas there is an efficiency plateau for a substrate temperature around 200 °C. For significantly higher substrate temperatures such as 240 °C there is a decrease in the efficiency values again. The difference in efficiency is mainly affected by the *V*_{OC} whereas FF and *J*_{SC} have minor influence. The increase in the scattering of efficiency data for solar cells fabricated with In_xS_y sputtered at temperatures lower and higher than 220 °C is mainly driven by the FF.

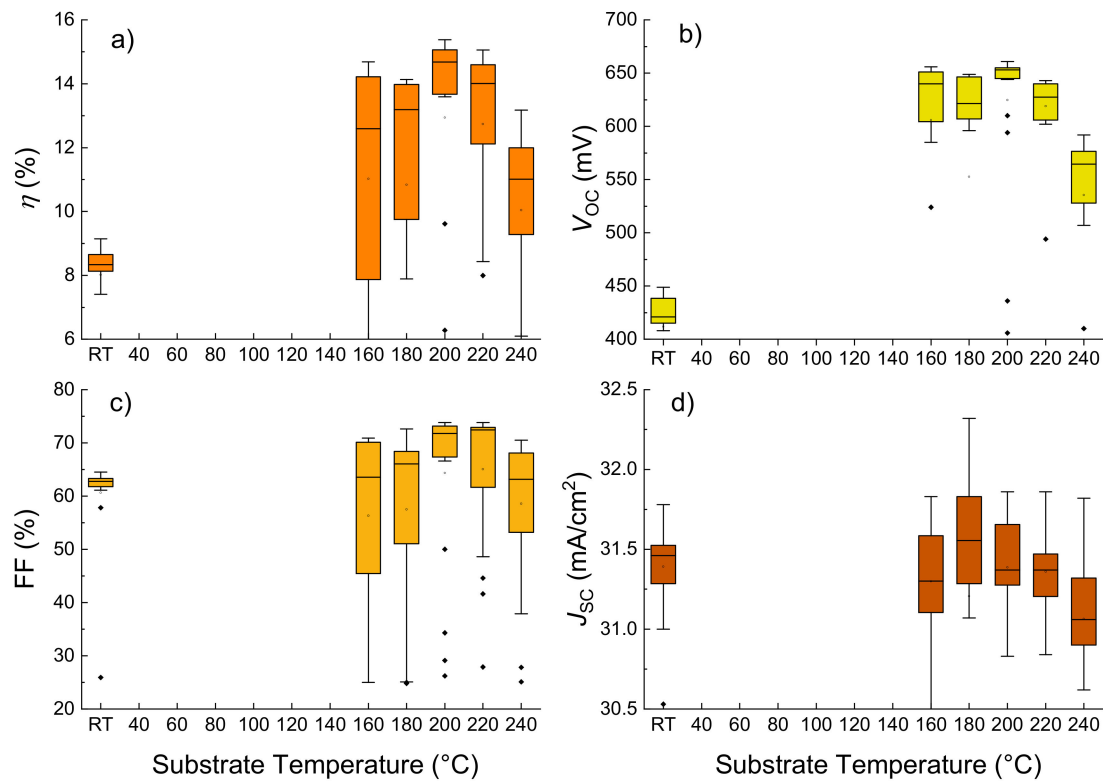


Figure 2. Solar cell parameters of CIGS thin-film solar cells with 60 nm thick In_xS_y buffer layers sputtered at different substrate temperatures. For each substrate temperature 20 solar cells were measured: (a) Power conversion efficiency η ; (b) Open circuit voltage V_{OC} ; (c) Fill factor FF; (d) Short-circuit current density J_{SC} .

3.2. Analysis of In_xS_y Layers and CIGS/Buffer Interface

3.2.1. Crystal Structure and Bandgap Energy of Sputtered In_xS_y

Figure 3a depicts the GIXRD patterns obtained on 500 nm thick In_xS_y layers on glass substrates. Both layers deposited at RT and 220 °C are crystalline and exhibit the tetragonal $\beta\text{-In}_2\text{S}_3$ structure [PDF no. 96-400-0814]. It should be noted that the reflexes of the cubic high-temperature structure [PDF no. 96-151-8188] overlap with most of the tetragonal reflexes, and Soni et al. reported recently the formation of cubic In_2S_3 by sputtering [12]. Therefore, a coexistence of this cubic α -phase could not be totally excluded in our case and probably this phase could occur in case there are locally very high temperatures above 717 K [13]. Even the sputtering power (density) [14] and thickness of the In_xS_y layers [15] could influence the structural properties of the deposited In_xS_y films. The high-temperature modification $\gamma\text{-In}_2\text{S}_3$ which typically forms for temperatures above 1049 K, as reported by Pistor et al. [13] is very unlikely to occur during our sputtering conditions.

Figure 3b illustrates the difference in transmittance of In_xS_y films deposited at RT and 220 °C under otherwise identical conditions on suprasil quartz glass substrates. The evaluated thicknesses from these transmittance measurements are 490 and 480 nm for RT and 220 °C, respectively. Thus, there is only a slight reduction in the sputter deposition rate with temperature. The main finding is that the optical absorption edge slightly shifts to higher energies for the sample with the In_xS_y buffer deposited at 220 °C. According to a model with an indirect bandgap energy (E_g) for In_2S_3 the values of $E_g = 2.02$ eV (RT) and $E_g = 2.08$ eV (220 °C), respectively, were extracted by extrapolation of the linear region in the $\sqrt{\alpha E}$ - E -plot, as illustrated in Figure 3c. In case a model with a direct bandgap E_g is used for the evaluation (not shown here), higher E_g values would result but with the same trend—a slight increase in E_g with elevated temperature. However, the corresponding $(\alpha E)^2$ - E -plots show no distinct linear shape as expected for a semiconductor with a direct bandgap. Generally, an increase in

bandgap energy might be expected as a result of the incorporation of oxygen in In_2S_3 [16]. In our case, this oxygen could probably stem from oxygen/water residual from the sputtering system, which could be more easily incorporated in the growing In_xS_y film deposited at higher substrate temperatures. Nevertheless, we could not clearly detect a higher amount of oxygen inside the In_xS_y layer grown at higher temperatures as reported in Section 3.2.2. A more likely explanation could be changes in chemical composition, i.e., in the sulfur/indium ratio as also shown Section 3.2.2.

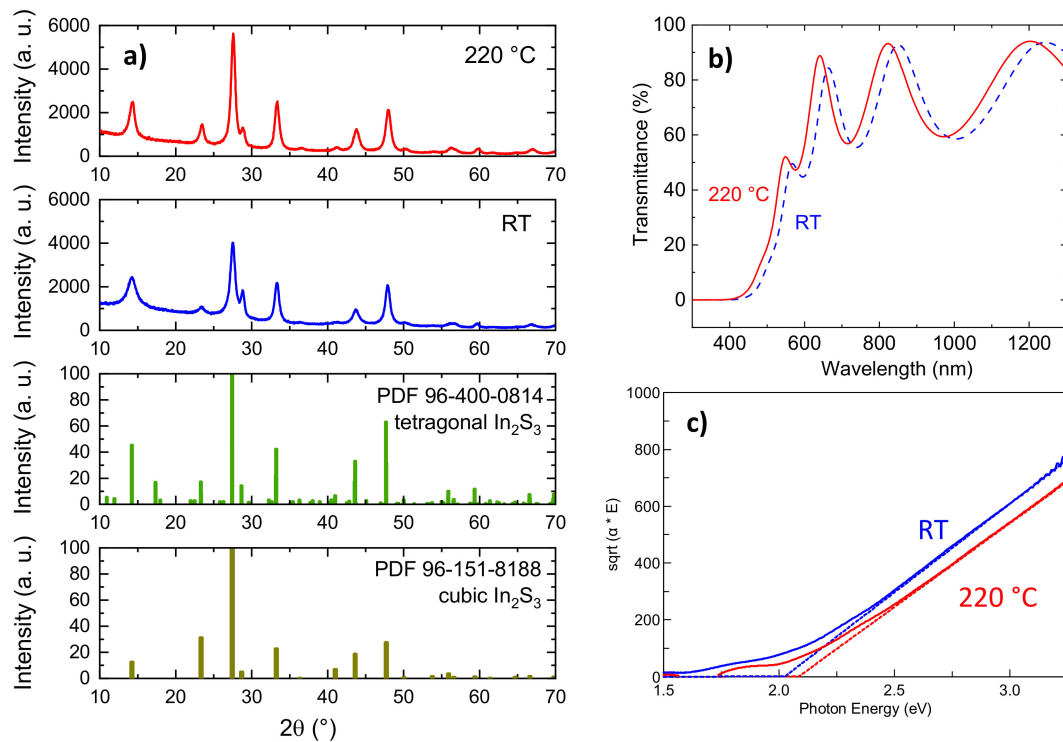


Figure 3. (a) GIXRD patterns measured with an incident angle of 0.5° on approximately 500 nm thick In_xS_y layers on suprasil quartz glass; (b) Transmittance measurement of about 500 nm thick In_xS_y layers on suprasil quartz glass; (c) Corresponding $\text{sqrt}(\alpha E)$ - E -plot (indirect bandgap energy for extraction of E_g value was used).

As a conclusion, only slight differences in structural and optical material properties between both In_2S_3 layers sputtered at RT and 220 °C were observed, which is an indication that pronounced changes in solar cell performance could be more affected by the interface formation between CIGS absorber and In_xS_y buffer layer.

3.2.2. Chemical Composition of In_xS_y /CIGS Interface Region

Depth profiles were performed by ToF-SIMS in order to get an idea what influences the efficiency and V_{OC} and to reveal changes in the chemical composition of the In_xS_y buffer and CIGS/buffer interface due to the different substrate temperatures during In_xS_y sputtering.

The quantified ToF-SIMS depth profiles shown in Figure 4 highlight changes in the chemical composition of the In_xS_y buffer layer deposited on CIGS. The chemical composition of In_xS_y grown at RT is stoichiometric, i.e., the layer has a homogeneous In_2S_3 composition over the whole 60 nm thickness; whereas for substrate temperatures higher than 200 °C, the In_xS_y composition becomes more sulfur-rich and indium-deficient, and the layers tend to be more inhomogeneous. ToF-SIMS depth profiles obtained on samples sputtered at 160 and 180 °C (omitted here for clarity) reflect the same trend as the RT sample.

Since pure argon without any addition of oxygen was used as sputtering gas, the oxygen concentration in all layers is expectedly very low, i.e., the S/(S+O) ratio is close to 1, indicating that no

oxygen is incorporated during the sputtering process even at the higher substrate temperatures of 220 and 240 °C. Small amounts of oxygen are only detected at the In_xS_y surface.

In addition to changes in the composition of the In_xS_y buffer, there is a pronounced copper depletion of the CIGS surface, which is more obvious for layers deposited at higher substrate temperatures of 220 and 240 °C compared to RT, 160, 180, and 200 °C. In a more detailed consideration, the copper depletion at the CIGS surface was estimated to rise from around 10 nm at RT, up to approximately 70 nm at 240 °C.

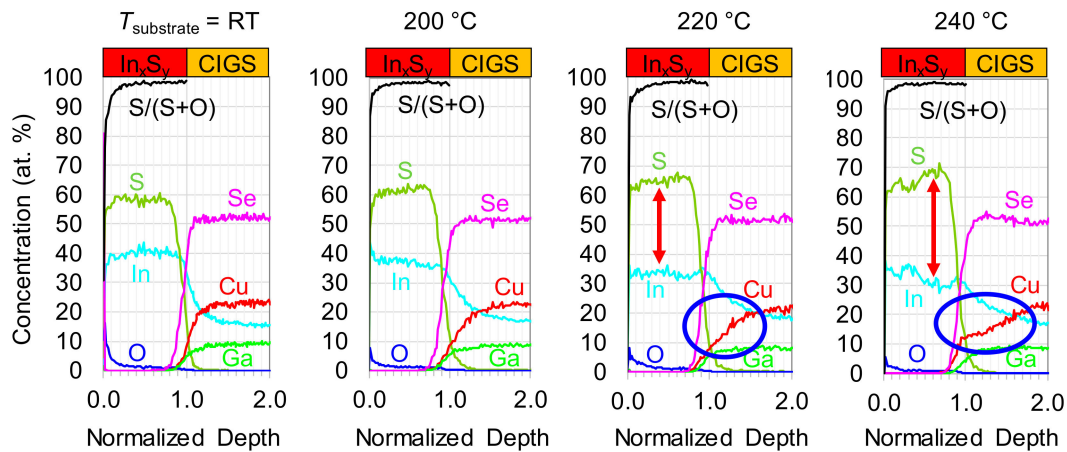


Figure 4. Quantified ToF-SIMS depth profiles performed with cesium cluster source for sputtering on $\text{In}_x\text{S}_y/\text{CIGS}$ samples deposited at different substrate temperatures ($T_{\text{substrate}}$) during In_xS_y sputtering. The x-axes are normalized for clarity. Nominal thickness of In_xS_y layers is 60 nm and sputtering inside CIGS was carried out within the first 100 nm. Changes in In_xS_y chemical composition are highlighted with red arrows and copper depletion of CIGS absorber is marked with blue circles.

ToF-SIMS depth profiles were also performed on complete CIGS solar cells from ZnO:Al front contact down to the soda-lime glass substrate to reveal differences in chemical composition between CIGS solar cells with efficiencies of 7.1% and 14.6% with In_xS_y buffer layers sputtered at RT and at 220 °C, respectively (Figure 5). The depth profile for the sample fabricated at higher substrate temperature exhibits a strong increase in the sodium signal inside the In_xS_y buffer layer and at the CIGS/buffer interface (note the logarithmic scale here). The sodium is originally diffusing from the soda-lime glass substrate through the molybdenum back contact into the CIGS layer at elevated deposition temperatures during the CIGS co-evaporation process but was not intentionally incorporated into the CIGS absorber or In_xS_y buffer layer.

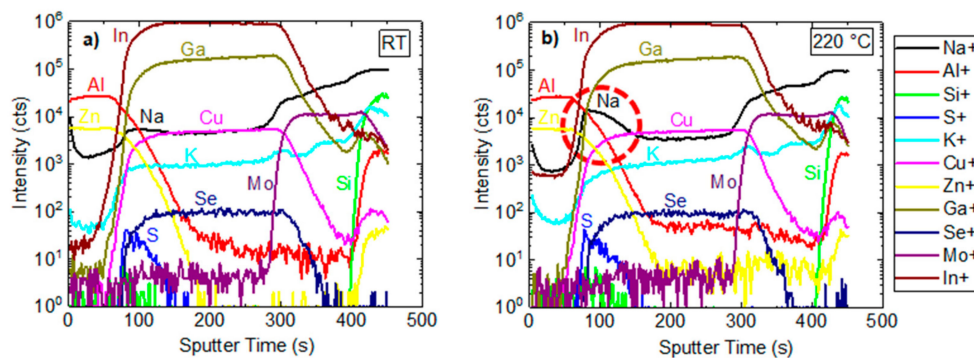


Figure 5. ToF-SIMS depth profiles performed with oxygen sputtering source on complete CIGS solar cells with stacking sequence ZnO:Al/i-ZnO/ In_xS_y /CIGS/Mo/glass. (a) Solar cell with 7.1% efficiency and In_xS_y buffer deposited at RT; (b) Solar cell with 14.6% efficiency and In_xS_y sputtered at 220 °C substrate temperature. The enhanced sodium signal is highlighted with a dashed red circle.

The observed sodium accumulation combined with a moderate copper depletion at the CIGS/ In_xS_y interface region could be the most significant effect for an efficiency improvement of In_2S_3 buffered CIGS-based solar cells.

4. Discussion

We have demonstrated that we could achieve suitable film quality for In_xS_y buffer layers with the very fast deposition method of rf-magnetron sputtering applied to CIGS thin-film solar cells to realize efficiencies above 15%. For our sputtered buffer layers, we applied high sputtering deposition rates around 0.8 nm/s; compared to slower deposition processes such as ALD, CBD, ILGAR, and thermal evaporation. Nevertheless, there is still an efficiency gap compared to the CdS-buffered reference cells, which was also observed in our previous works with sputtered In_xS_y buffers [10,17] and reported by other groups for CIGS cells with sputtered In_xS_y buffers [12,18,19], evaporated In_xS_y buffers [20,21], and our own cells with In_xS_y layers grown by metal-organic chemical vapor deposition [22].

For both 500 nm thick In_xS_y layers deposited at RT and 220 °C substrate temperature on glass substrates, we obtained crystalline structures without any huge difference between both layers. We indicated the tetragonal β -phase for In_2S_3 . This result is in accordance with structural investigations on rf-sputtered In_xS_y layers reported by other groups [14,15,23], but also for structural investigations on evaporated In_xS_y layers [20,24]. In contrast, high-resolution transmission electron microscopy analyses revealed nanocrystalline structures for our oxygen-containing CBD- $\text{In}_x(\text{O},\text{S})_y$ [25] and sputtered $\text{In}_x(\text{O},\text{S})_y$ buffer layers deposited from an $\text{In}_2(\text{O}_{0.25}\text{S}_{0.75})_3$ target [26] at the CIGS/buffer interface in the complete device.

The extracted bandgap energy (indirect) for our In_xS_y is in the range of 2.0–2.1 eV, thus not perfectly ideal for an application as a buffer in CIGS thin-film solar cells. With the addition of dopants like chlorine [8], oxygen [16], or sodium [1], the bandgap energy can be increased to suitable values to reduce parasitic absorption of the buffer and obtain high J_{SC} . In addition, a beneficial band alignment with chalcopyrite-based absorber is necessary to obtain high V_{OC} [27] and close the efficiency gap to the CdS-buffered reference cells. In this sense, the surface termination of the CIGS absorber could play an important role. The parasitic absorption can be also reduced by using thinner In_xS_y buffers with thicknesses below 20 nm. In this case the subsequent high-resistive layer becomes more important in terms of band alignment. It should be noted that the power density during sputtering could influence the bandgap value of In_xS_y layers as well [14]. Our extracted bandgap energy increases slightly around 0.06 eV with the substrate temperature during In_xS_y sputtering. This trend with increasing temperature was also observed by other groups for sputtered In_xS_y layers [17,18,28]. In contrast, Karthikeyan et al. reported an opposite trend as found for their In_xS_y deposited by pulsed direct magnetron sputtering [23]. From theoretical density calculations there is only a very small difference between direct and indirect transitions in β - In_2S_3 [29,30].

The substrate temperature during In_xS_y sputtering has a major influence on the performance of the device. Solar cells with In_xS_y sputtered at RT result in poor efficiencies whereas a maximum seems to be around 200 °C. For higher temperatures >240 °C, there is a decrease in efficiency and V_{OC} again. The strong dependency of solar cell efficiency on substrate temperature during sputtering and sample pre-conditioning was also observed in previous experiments at ZSW [10,17] and by other groups [31]. For higher substrate temperatures above 220 °C there seems to be a destruction of the important pn-junction at the CIGS/buffer interface resulting in deteriorated solar cell parameters.

In addition, the substrate temperature during In_xS_y sputtering has an influence on the chemical composition of the In_xS_y buffer and CIGS/buffer interface. In this work, we observed an increasing sulfur/indium ratio starting from a value of 3:2 (In_2S_3) grown at RT with increasing substrate temperature during sputtering, similar to the trend in our previous experiments, but with a different starting ratio of around 1:1 [17], and similar to results obtained by D. Abou-Ras et al. [31].

The sodium accumulation in the In_xS_y buffer and at the CIGS/buffer interface and the copper-depleted CIGS surface seem to be the most likely candidates to increase the V_{OC} of the

220 °C cell compared to the RT cell. Sodium addition to CIGS in general increases the V_{OC} , e.g., in case a sodium-free substrate is used and sodium is intentionally incorporated with a precursor [32] or post-deposition process [33]. Sodium accumulation in the buffer and at the CIGS/buffer interface was also found after post-annealing processes for CBD Zn(O,S)-buffered devices [34]. A sodium accumulation on the nano scale was observed by atom probe tomography measurements at the CIGS/ In_xS_y interface for samples annealed at temperatures above 225 °C compared to the RT samples without sodium accumulation [12]. The observed copper depletion at the CIGS surface could result in an ordered vacancy compound with a slightly higher bandgap due to a lowered valence band maximum. This feature could promote an improved band alignment in combination with the In_xS_y buffer and could be also a reason for improved V_{OC} values as reported for evaporated $In_xS_y:Na$ buffer on $Cu(In,Ga)(S,Se)_2$ [27]. The formation of such a Cu-poor $CuIn_5S_8$ composition at the CIGS/sputtered In_xS_y interface was observed at relatively high temperatures around 340 °C [31]. In general, the integral copper content of the CIGS absorber can significantly influence the efficiency and the dominating recombination mechanism of In_xS_y -buffered devices [35].

The phenomena of copper diffusion at the CIGS/ In_2S_3 interface, when investigated, was mostly isolated from alkali elements in the past. Pistor et al. clearly showed with high kinetic energy X-ray photoelectron spectroscopy that above 200 °C, the copper diffusion from CIGS into In_2S_3 is enhanced [36]. Recent calculations with density functional theory also took sodium into account and revealed an interplay between sodium and copper diffusion at the CIGS/ In_2S_3 interface, and the formation of Na- and Cu-containing phases is very likely due to strong negative driving force energies (energy releasing processes). The even lower driving force energy value for sodium implies that sodium diffusion is more favored than copper diffusion and would therefore be actuated earlier [37]. This difference could be one explanation for our observed results from the depth profiles: First, there is a sodium diffusion up to 200 °C with only small changes in copper. For higher temperatures >220 °C the copper diffusion is no longer hindered by the sodium and copper diffusion takes place. Following this argumentation, the important parameter for an increased efficiency is the sodium accumulation at the CIGS/buffer interface and a moderate copper depletion at the CIGS surface. An enhanced copper enrichment of the In_2S_3 layer would be detrimental. It should be noted that, besides the copper depletion of the CIGS surface, an intermixing between In_xS_y buffer and CIGS absorber could also take place. A possible sulfur incorporation into the CIGS absorber, which we did not observe clearly in the ToF-SIMS profiles, would lead to a lowered valence band maximum and a different band alignment to In_xS_y .

Future research directions could address one or several of the following approaches: Sodium can be intentionally inserted in the In_2S_3 target to increase the bandgap energy, similar to the sodium-containing In_xS_y buffer used by the company Avancis deposited by thermal evaporation [7]. In addition, post-annealing procedures or heat-light soaking could be an adequate approach to diffuse sodium into the In_xS_y buffer and to the CIGS/buffer interface, which was already successfully applied to CIGS cells with CBD-Zn(O,S)/(Zn,Mg)O buffer system. Oxygen can be intentionally introduced via reactive sputtering with oxygen in the sputtering gas [2], via variation of the base pressure with water vapor as oxygen source [18], the use of mixed $In_2(O,S)_3$ targets, or co-sputtering from pure In_2S_3 and In_2O_3 targets. Another approach could be the use of a very thin In_xS_y layer with a thickness of 20 nm or even less. In this case the subsequent high-resistive layer should be optimized, e.g., (Zn,Mg)O or $ZnTiO_x$ [38] could be candidates to replace *i*-ZnO. Furthermore, different window layers—such as $InZnO_x$ or $InSnO_x$ instead of ZnO:Al—can influence the device performance of CIGS solar cells in combination with sputtered $In_x(O,S)_y$ buffers [2].

5. Conclusions

The substrate temperature during the sputtering of In_xS_y buffer layers significantly influences the performance of CIGS thin-film solar cells. The best power conversion efficiencies in the as-grown state were obtained at a temperature plateau around 200 °C with the best value of 15.3% compared to the

reference cell with solution-grown CdS buffer with 17.1% efficiency. The difference in performance compared to cells with buffers deposited below 200 °C is mainly due to a reduced V_{OC} . The chemical composition and homogeneity of In_xS_y changes from stoichiometric and homogenous In_2S_3 for layers deposited RT to inhomogenous and more sulfur-rich and indium-deficient composition for higher temperatures in the range of 220–240 °C. In addition, there is a pronounced copper depletion at the CIGS absorber surface and a sodium accumulation in the In_xS_y buffer and at the CIGS/buffer interface for higher temperatures compared to In_xS_y layers deposited at RT. These two features could explain the higher V_{OC} values of cells with In_xS_y buffers grown at higher substrate temperatures compared to RT. However, In_xS_y layers with a non-ideal bandgap energy of 2.0–2.1 eV (indirect) induce parasitic losses and a limited J_{SC} . In future research, appropriate quantities of sodium and/or oxygen could be intentionally incorporated in the In_xS_y layer and—with very thin In_xS_y layers, in combination with an optimized high-resistive layer—the parasitic absorption could be further reduced and the J_{SC} increased.

Author Contributions: Conceptualization, D.H. and W.W.; validation, D.H., W.H., R.M. and W.W.; investigation, D.H., W.H., R.M., and W.W.; writing—original draft preparation, W.W.; writing—review and editing, D.H., W.H., R.M., and W.W.; visualization, D.H.; project administration, W.W.; funding acquisition, W.W. All authors have read and agreed to the published version of the manuscript.

Funding: This research was funded by the German Federal Ministry for Economic Affairs and Energy (BMWi) within the “EFFCIS” project under contract number 0324076A.

Acknowledgments: We thank the CIGS team at ZSW for solar cell preparation, especially Stefan Paetel for CIGS deposition.

Conflicts of Interest: The authors declare no conflict of interest. The funders had no role in the design of the study; in the collection, analyses, or interpretation of data; in the writing of the manuscript, or in the decision to publish the results.

References

1. Palm, J.; Dalibor, T.; Lechner, R.; Pohlner, S.; Verma, R.; Dietmüller, R.; Heiß, A.; Vogt, H.; Karg, F. Cd-free CIS thin film solar modules at 17% efficiency. In Proceedings of the 29th European Photovoltaic Solar Energy Conference, Amsterdam, The Netherlands, 22–26 September 2014; pp. 1433–1438.
2. Niemi, E.; Sterner, J.; Carlsson, P.; Oliv, J.; Jaremalm, E.; Lindström, S. All-sputtered flexible CIGS cells at high speed. In Proceedings of the 31st European Photovoltaic Solar Energy Conference, Hamburg, Germany, 14–18 September 2015; pp. 1010–1013.
3. Barreau, N. Indium sulfide and relatives in the world of photovoltaics. *Sol. Energy* **2009**, *83*, 363–371. [[CrossRef](#)]
4. Naghavi, N.; Abou-Ras, D.; Allsop, N.; Barreau, N.; Bücheler, S.; Ennaoui, A.; Fischer, C.-H.; Guillen, C.; Hariskos, D.; Herrero, J.; et al. Buffer layers and transparent conducting oxides for chalcopyrite $Cu(In,Ga)(S,Se)_2$ based thin film photovoltaics: Present status and current developments. *Prog. Photovolt. Res. Appl.* **2010**, *18*, 411–433. [[CrossRef](#)]
5. Mughal, M.A.; Engelken, R.; Sharma, R. Progress in indium (III) sulfide (In_2S_3) buffer layer deposition techniques for CIS, CIGS, and CdTe-based thin film solar cells. *Sol. Energy* **2015**, *120*, 131–146. [[CrossRef](#)]
6. Spiering, S.; Nowitzki, A.; Kessler, F.; Igalson, M.; Maksoud, H.A. Optimization of buffer-window layer system for CIGS thin film devices with indium sulphide buffer by in-line evaporation. *Sol. Energy Mater. Sol. Cells* **2016**, *144*, 544–550. [[CrossRef](#)]
7. Dalibor, T.; Eraerds, P.; Grave, M.; Algasinger, M.; Visbeck, S.; Niesen, T.; Palm, J. Advanced PVD buffers on the road to GW-scale CIGS_{Se} production. In Proceedings of the 43rd IEEE Photovoltaics Specialists Conference, Portland, OR, USA, 5–10 June 2016; pp. 1433–1437.
8. Sáez-Araoz, R.; Krammer, J.; Harndt, S.; Koehler, T.; Krueger, M.; Pistor, P.; Jasenek, A.; Hergert, F.; Lux-Steiner, M.C.; Fischer, C.-H. ILGAR In_2S_3 buffer layers for Cd-free $Cu(In,Ga)(S,Se)_2$ solar cells with certified efficiencies above 16%. *Prog. Photovolt. Res. Appl.* **2012**, *20*, 855–861. [[CrossRef](#)]
9. Voorwinden, G.; Kniese, R.; Jackson, P.; Powalla, M. In-Line $Cu(In,Ga)Se_2$ co-evaporation process on 30 cm × 30 cm substrates with multiple deposition stages. In Proceedings of the 22nd European Photovoltaic Solar Energy Conference, Milan, Italy, 3–7 September 2007; pp. 2115–2118.

10. Hariskos, D.; Menner, R.; Spiering, S.; Eicke, A.; Powalla, M.; Ellmer, K.; Oertel, M.; Dimmler, B. In₂S₃ Buffer layer deposited by magnetron sputtering for Cu(In,Ga)Se₂ solar cells. In Proceedings of the 19th European Photovoltaic Solar Energy Conference, Paris, France, 7–11 June 2004; pp. 1894–1897.
11. Kluth, O.; Schöpe, G.; Rech, B.; Menner, R.; Oertel, M.; Orgassa, K.; Schock, H.W. Comparative material study on RF and DC magnetron sputtered ZnO:Al films. *Thin Solid Films* **2006**, *502*, 311–316. [[CrossRef](#)]
12. Soni, P.; Raghuwanshi, M.; Wuerz, R.; Berghoff, B.; Knoch, J.; Raabe, D.; Cojocar-Mirédin, O. Role of elemental intermixing at the In₂S₃/CIGSe heterojunction deposited using reactive RF magnetron sputtering. *Sol. Energy Mater. Sol. Cells* **2019**, *195*, 367–375. [[CrossRef](#)]
13. Pistor, P.; Merino Álvarez, J.M.; León, M.; di Michiel, M.; Schorr, S.; Klenk, R.; Lehmann, S. Structure reinvestigation of α -, β - and γ -In₂S₃. *Acta Crystallogr. B Struct. Sci. Cryst. Eng. Mater.* **2016**, *B72*, 410–415. [[CrossRef](#)]
14. Hwang, D.H.; Cho, S.; Hui, K.N.; Son, Y.G. Effect of sputtering power on structural and optical properties of radio frequency-sputtered In₂S₃ thin films. *J. Nanosci. Nanotechnol.* **2014**, *14*, 8978–8981. [[CrossRef](#)]
15. Ji, Y.; Ou, Y.; Yu, Z.; Yan, Y.; Wang, D.; Yan, C.; Liu, L.; Zhang, Y.; Zhao, Y. Effect of film thickness on physical properties of RF sputtered In₂S₃ layers. *Surf. Coat. Technol.* **2015**, *276*, 587–594. [[CrossRef](#)]
16. Barreau, N.; Bernède, J.C.; Marsillac, S.; Mokrani, A. Study of low temperature elaborated tailored optical band gap β -In₂S_{3-3x}O_{3x} thin films. *J. Cryst. Growth* **2002**, *235*, 439–449. [[CrossRef](#)]
17. Hariskos, D.; Menner, R.; Lotter, E.; Spiering, S.; Powalla, M. Magnetron sputtering of indium sulphide as the buffer layer in Cu(In,Ga)Se₂-based solar cells. In Proceedings of the 20th European Photovoltaic Solar Energy Conference, Barcelona, Spain, 6–10 June 2005; pp. 1713–1716.
18. Ho, W.-H.; Hsu, C.-H.; Wei, S.-Y.; Cai, C.-H.; Huang, W.-C.; Lai, C.-H. Sputtered In_x(O,S)_y buffer layers for Cu(In,Ga)Se₂ thin-film solar cells: Engineering of band alignment and interface properties. *ACS Appl. Mater. Interfaces* **2017**, *9*, 17586–17594. [[CrossRef](#)] [[PubMed](#)]
19. Soni, P.; Raghuwanshi, M.; Wuerz, R.; Berghoff, B.; Knoch, J.; Raabe, D.; Cojocar-Mirédin, O. Sputtering as a viable route for In₂S₃ buffer layer deposition in high efficiency Cu(In,Ga)Se₂ solar cells. *Energy Sci. Eng.* **2019**, *7*, 478–487. [[CrossRef](#)]
20. Pistor, P.; Caballero, R.; Hariskos, D.; Izquierdo-Roca, V.; Wächter, R.; Schorr, S.; Klenk, R. Quality and stability of compound indium sulphide as source material for buffer layers in Cu(In,Ga)Se₂ solar cells. *Sol. Energy Mater. Sol. Cells* **2009**, *93*, 148–152. [[CrossRef](#)]
21. Verma, R.; Datta, D.; Chirila, A.; Güttler, D.; Perrenoud, J.; Pianezzi, F.; Müller, U.; Kumar, S.; Tiwari, A.N. Optical, structural, and chemical properties of flash evaporated In₂S₃ buffer layer Cu(In, Ga)Se₂ for solar cells. *J. Appl. Phys.* **2010**, *108*, 074904. [[CrossRef](#)]
22. Spiering, S.; Bürkert, L.; Hariskos, D.; Powalla, M.; Dimmler, B.; Giesen, C.; Heuken, M. MOCVD indium sulphide for application as a buffer layer in CIGS solar cells. *Thin Solid Films* **2009**, *517*, 2328–2331. [[CrossRef](#)]
23. Karthikeyan, S.; Hill, A.E.; Pilkington, R.D. Low temperature pulsed direct current magnetron sputtering technique for single phase β -In₂S₃ buffer layers for solar cell applications. *Appl. Surf. Sci.* **2017**, *418*, 199–206. [[CrossRef](#)]
24. Barreau, N.; Marsillac, S.; Albertini, D.; Bernede, J.C. Structural, optical and electrical properties of β -In₂S_{3-3x}O_{3x} thin films obtained by PVD. *Thin Solid Films* **2002**, *403–404*, 331–334. [[CrossRef](#)]
25. Jin, X.; Popescu, R.; Pasha, A.; Schneider, R.; Hariskos, D.; Witte, W.; Powalla, M.; Gerthsen, D. Structural and microchemical characterization of Cu(In,Ga)Se₂ solar cells with solution-grown CdS, Zn(O,S), and In_x(O,S)_y buffers. *Thin Solid Films* **2019**, *671*, 133–138. [[CrossRef](#)]
26. Jin, X.; Schneider, R.; Popescu, R.; Hariskos, D.; Witte, W.; Powalla, M.; Gerthsen, D. Characterization of solution-grown and sputtered In_x(O,S)_y buffer layers in Cu(In,Ga)Se₂ solar cells by analytical TEM. *J. Semicond. Sci. Technol.* **2020**, *35*, 034001. [[CrossRef](#)]
27. Hauschild, D.; Meyer, F.; Benkert, A.; Kreikemeyer-Lorenzo, D.; Dalibor, T.; Palm, J.; Blum, M.; Yang, W.; Wilks, R.G.; Bär, M.; et al. Improving performance by Na doping of a buffer layer—Chemical and electronic structure of the In_xS_y:Na/CuIn(S,Se)₂ thin-film solar cell interface. *Prog. Photovolt. Res. Appl.* **2018**, *26*, 359–366. [[CrossRef](#)]
28. Siol, S.; Dhakal, T.P.; Gudavalli, G.S.; Rajbhandari, P.P.; DeHart, C.; Baranowski, L.L.; Zakutayev, A. Combinatorial reactive sputtering of In₂S₃ as an alternative contact layer for thin film solar cells. *ACS Appl. Mater. Interfaces* **2016**, *8*, 14004–14011. [[CrossRef](#)] [[PubMed](#)]

29. Sharma, Y.; Srivastava, P. Electronic, optical and transport properties of α -, β - and γ -phases of spinel indium sulphide: An ab initio study. *Mater. Chem. Phys.* **2012**, *135*, 385–394. [[CrossRef](#)]
30. Ghorbani, E.; Erhart, P.; Albe, K. Energy level alignment of Cu(In,Ga)(S,Se)₂ absorber compounds with In₂S₃, NaIn₅S₈, and CuIn₅S₈ Cd-free buffer materials. *Phys. Rev. Mater.* **2019**, *3*, 075401. [[CrossRef](#)]
31. Abou-Ras, D.; Kostorz, G.; Hariskos, D.; Menner, R.; Powalla, M.; Schorr, S.; Tiwari, A.N. Structural and chemical analyses of sputtered In_xS_y buffer layers in Cu(In,Ga)Se₂ thin-film solar cells. *Thin Solid Films* **2009**, *517*, 2792–2798. [[CrossRef](#)]
32. Caballero, R.; Kaufmann, C.A.; Eisenbarth, T.; Unold, T.; Klenk, R.; Schock, H.-W. High efficiency low temperature grown Cu(In,Ga)Se₂ thin film solar cells on flexible substrates using NaF precursor layers. *Prog. Photovolt. Res. Appl.* **2011**, *19*, 547–551. [[CrossRef](#)]
33. Rudmann, D.; da Cunha, A.F.; Kaelin, M.; Kurdesau, F.; Zogg, H.; Tiwari, A.N.; Bilger, G. Efficiency enhancement of Cu(In,Ga)Se₂ solar cells due to post-deposition Na incorporation. *Appl. Phys. Lett.* **2004**, *84*, 1129–1131. [[CrossRef](#)]
34. Witte, W.; Hariskos, D.; Eicke, A.; Menner, R.; Kiowski, O.; Powalla, M. Impact of annealing on Cu(In,Ga)Se₂ solar cells with Zn(O,S)/(Zn,Mg)O buffers. *Thin Solid Films* **2013**, *535*, 180–183. [[CrossRef](#)]
35. Spiering, S.; Paetel, S.; Kessler, F.; Igalson, M.; Maksoud, H.A. Copper variation in Cu(In,Ga)Se₂ solar cells with indium sulphide buffer layer. *Thin Solid Films* **2015**, *582*, 328–331. [[CrossRef](#)]
36. Pistor, P.; Allsop, N.; Braun, W.; Caballero, R.; Camus, C.; Fischer, C.-H.; Gorgoi, M.; Grimm, A.; Johnson, B.; Kropp, T.; et al. Cu in In₂S₃: Interdiffusion phenomena analysed by high kinetic energy X-ray photoelectron spectroscopy. *Phys. Status Solidi A* **2009**, *5*, 1059–1062. [[CrossRef](#)]
37. Ghorbani, E.; Albe, K. Influence of Cu and Na incorporation on the thermodynamic stability and electronic properties of β -In₂S₃. *J. Mater. Chem. C* **2018**, *6*, 7226–7231. [[CrossRef](#)]
38. Löckinger, J.; Nishiwaki, S.; Andres, C.; Erni, R.; Rossell, M.D.; Romanyuk, Y.E.; Buecheler, S.; Tiwari, A.N. ALD-Zn_xTi_yO as window layer in Cu(In,Ga)Se₂ solar cells. *ACS Appl. Mater. Interfaces* **2018**, *10*, 43603–43609.



© 2020 by the authors. Licensee MDPI, Basel, Switzerland. This article is an open access article distributed under the terms and conditions of the Creative Commons Attribution (CC BY) license (<http://creativecommons.org/licenses/by/4.0/>).